JOURNAL OF AIRCRAFT
Vol. 47, No. 1, January–February 2010

Engineering Notes

Efficient Numerical Aeroelastic Analysis of a High-Aspect-Ratio Wing Considering Geometric Nonlinearity

Kyung-Seok Kim* and In Lee†
Korea Advanced Institute of Science and Technology, Daejeon 305-701, Republic of Korea
Jae-Han Yoo‡
Korea Aerospace Research Institute, Daejeon, 305 333, Republic of Korea
and
Hyun-Ki Lee§
Hyundai Kia Motors, Gyeonggi-Do 445-706, Republic of Korea

DOI: 10.2514/1.45406

Nomenclature

e_1, e_2, e_3	=	reference orthogonal unit vectors in the undeformed configuration
$\bar{e}_{11}, \bar{e}_{12}, \bar{e}_{13}$	=	strain vectors at the reference point
e_1^*, e_2^*, e_3^*	=	reference orthogonal unit vectors in the deformed configuration
i_1, i_2, i_3	=	fixed orthogonal unit vectors
$\kappa_1, \kappa_2, \kappa_3$	=	strain curvature vectors in the undeformed configuration
q	=	generalized nodal displacement vector
$T(x_1)$	=	transformation matrix between a deformed-beam axis and a reference beam axis
$t_e(x_1)$	=	transformation matrix between an undeformed-beam axis and a deformed-beam axis
u, v, w	=	elastic displacements in the x, y, and z directions, respectively
w_1, w_2, w_3	=	warping displacement
γ	=	specific heat ratio
θ_0	=	steady angle of attack at root section
ϕ	=	disturbance velocity potential

I. Introduction

Predictions of aeroelastic stability for a high-altitude, long-endurance (HALE) aircraft have been studied in recent years. HALE aircraft are used for a variety of flight missions, including those related to unmanned reconnaissance, long-term surveillance, environmental sensing, and communication relay. For these types of missions, it is necessary for a wing to have a high lift-to-drag ratio and a lightweight structure. Thus, the wing of the HALE aircraft is designed in consideration of a high-aspect-ratio-wing concept. For example, the wing of HALE has an aspect ratio of approximately 35 and uses highly flexible structures. Because of these wing characteristics, a large deflection of the wing tip of nearly 25% of the wing semispan can occur. Such a large deflection can be categorized as a type of geometric structural nonlinearity. For several decades, aeroelastic analyses that take into account a geometric structural nonlinearity have been conducted on the rotor blades of helicopters. For the aeroelasticity of a rotary wing, aeroelastic stability can be affected by geometric structural nonlinearity. In general, a blade is modeled by using a beam to consider the geometrical nonlinearity. In the field of fixed-wing aeroelasticity, the aeroelastic characteristics of high-aspect-ratio wings are investigated using a beam model. Van Schoor and von Flotow [1] investigated aeroelastic characteristics using a human-powered aircraft model. A complete aircraft was modeled using a few modes of vibration, including rigid-body modes. In addition, the doublet-lattice theory was applied to an aerodynamic model. Pendaries [2] showed the results of a linear aeroelastic flight dynamic analysis. However, both of these studies were performed under the assumption of a linear structural model. Thus, the effects of geometric structural nonlinearity were not considered in the aeroelastic analyses. Recently, however, Patil et al. [3,4] investigated the static and dynamic aeroelastic characteristics of a high-aspect-ratio wing. For a structural analysis, the wing is modeled by a beam, and the effects of the geometric structural nonlinearity are described by using the Rodrigues parameter, which represents a rotation. For nonlinear aerodynamic loads, finite-state unsteady aerodynamics using a stall model was applied in their research. The results indicate that the flutter characteristics change due to geometric structural nonlinearity. Hall et al. [5] presented a study that combined three-dimensional nonplanar aerodynamic theory and a linear structural analysis. The instability of the flutter speed was reduced through the curvature of the wing. Theoretical and experimental investigations of flutter and limit cycle oscillations using a nonlinear beam model and the ONERA stall model were conducted by Tang and Dowell [6]. Patil and Hodges [7] developed an aeroelastic analysis using a nonlinear structural model with three-dimensional aerodynamics. For a static aeroelastic analysis, vortex-lattice method, which includes the curvature of the wing, was applied. On the other hand, double-lattice method was used for a dynamic aeroelastic analysis. It was found that the flutter stability values, which are obtained by two different aerodynamic methods, are similar to each other. More recently, Smith et al. [8] performed a static aeroelastic analysis based on computational fluid dynamics (CFD). The Euler equation and a geometrically exact beam model were used in their research. In addition, aeroelastic analyses of highly flexible wings were done by coupling the Navier–Stokes equation with nonlinear beam finite elements [9].

In the aforementioned studies, the aerodynamic models used panel methods or Euler/Navier–Stokes equations for the aeroelastic analyses. However, it is difficult to consider the effect of a camber and a thickness of a wing when using these methods with linear aerodynamic models. On the other hand, Euler/Navier–Stokes equations are inefficient for three-dimensional configurations due to the high computational cost associated with these equations. Thus, an efficient aeroelastic method is presented to include both geometrical structural and aerodynamic nonlinearities in this research. The transonic-small-disturbance theory (TSD) is well known as an efficient method for aeroelastic analysis. The TSD theory can simply create a computational mesh and is known for its efficient computing time. Hence, to

Received 12 May 2009; revision received 29 September 2009; accepted for publication 12 October 2009.

*Graduate Research Assistant, Department of Aerospace Engineering, 335 Gwahangno, Yuseong-gu.
†Professor, Department of Aerospace Engineering, 35 Gwahangno, Yuseong-gu. Associate Fellow AIAA.
‡Senior Researcher, Future Launch Vehicle Technology Department, 115 Gwahangno, Yuseong-gu.
§Research Engineer, Corporate Research and Development Division, 772-1, Jangduk-Dong, Hwaseong-Si.

achieve the goal of this study, aeroelastic analyses of a HALE aircraft wing are performed using the TSD theory and large-deflection-beam theory for an aerodynamic and a structural analysis, respectively. For the aeroelastic analysis, a nonlinear structural solver based on a finite element method is directly coupled with a fluid solver. For the geometric structural nonlinearity, a finite element approach using a large deflection beam is applied for the geometric structural nonlinear effect. The structural model used in the present analysis is a modified form of the beam model by Bauchau and Hong [10]. Additionally, a structural mesh and a CFD grid do not coincide with each other. Transformation methods of displacements from the finite element method (FEM) mesh to the CFD grid and forces from the CFD grid to the FEM mesh are considered.

II. Theoretical Background

A. Large-Deflection-Beam Theory

To analyze the nonlinear beam model, the geometry and coordinate systems under large deformation are illustrated in Fig. 1. Here, the triad i_1, i_2, and i_3 are fixed in a reference frame; the triad e_1, e_2, and e_3 is attached to a reference line along the axis of the undeformed beam; and the triad e_1^*, e_2^*, and e_3^* is attached to a reference line along the axis of the deformed beam. The geometrical nonlinearities are expressed using coordinate transformation matrices with the Euler angles in the present larger-deflection-beam theory:

$$e_i^* = t_e(x_1)e_i = T(x_1)i_i, \quad \text{where } T(x_1) = t_e(x_1)t_g(x_1) \tag{1}$$

The transformation matrices t_g, t_e, and T depend on the curvilinear axial coordinate x_1. Assuming that the initial curvature values are small and that the shearing strains are smaller than unity in the Green–Lagrangian strain components, the strain-displacement relationships are represented as given in [11]. The strain-displacement relationships are given in [12].

$$\begin{aligned} \varepsilon_{11} &= \bar{e}_{11} + x_3\kappa_2 - x_2\kappa_3 + w_1', \qquad \varepsilon_{22} = w_{2,2}, \qquad \varepsilon_{33} = w_{3,3} \\ \gamma_{12} &= 2\bar{e}_{12} - x_3\kappa_1 + w_{1,2} + w_2', \qquad \gamma_{23} = w_{2,3} + w_{3,2} \\ \gamma_{13} &= 2\bar{e}_{13} + x_2\kappa_1 + w_{1,3} + w_3' \qquad \kappa_i = K_i - k_i \end{aligned} \tag{2}$$

Here, x_1, x_2, and x_3 are curvilinear coordinates. w_1, w_2 and w_3 are the general warping displacements of an arbitrary point on the cross section. The force-strain ($\bar{e}_{11}, 2\bar{e}_{12}$, and $2\bar{e}_{13}$) and moment-strain (κ_1, κ_2, and κ_3) components are given in the literature [13]. Herein, prime denotes the derivative with respect to x_1 and i denotes the derivatives with respect to x_i ($i = 2, 3$). Using Hamilton's principle, the equation of motion can be obtained as

$$\int_{t_1}^{t_2} (\delta U - \delta T - \delta W)\, \mathrm{d}t = 0 \tag{3}$$

where

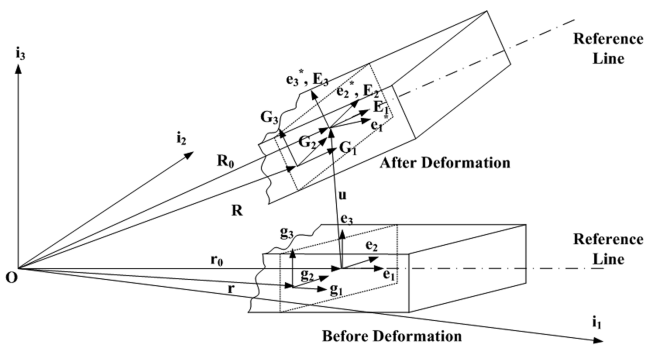

Fig. 1 Geometry and coordinate systems under large deformation.

$$\delta U = \int_0^l \delta \begin{Bmatrix} \bar{\mathbf{e}} \\ \bar{\boldsymbol{\kappa}} \end{Bmatrix} \begin{bmatrix} \mathbf{A} & \mathbf{B} \\ \mathbf{B}^T & \mathbf{D} \end{bmatrix} \begin{Bmatrix} \bar{\mathbf{e}} \\ \bar{\boldsymbol{\kappa}} \end{Bmatrix} \mathrm{d}x_1$$

$$\delta T = \int_0^l \int_A \rho \{\delta \mathbf{V}_i\}^T \{\mathbf{V}_i\}\, \mathrm{d}A\, \mathrm{d}x_1$$

$$\delta W = \int_0^l \int_A \delta \{\mathbf{R}_i\}^T \{\mathbf{f}_i\}\, \mathrm{d}A\, \mathrm{d}x_1$$

Here, δU, δT, and δW are the variation of the strain energy, the variation of the kinetic energy, and the virtual work done by external forces. The sectional stiffness matrices $\mathbf{A}$, $\mathbf{B}$, and $\mathbf{D}$ are 3×3 matrices that depend not only on the material properties but also on the cross-sectional geometry, initial curvature, and twists. In the case of an isotropic material, these matrices are represented by the diagonal term [13]. The nonlinear finite element equation of motion is obtained in the matrix form of

$$[\mathbf{M}(\mathbf{q})]\{\ddot{\mathbf{q}}\} + \mathbf{P}(\mathbf{q}) - \mathbf{P}_A(\mathbf{q}) = \{0\} \tag{4}$$

where $\mathbf{M}(\mathbf{q})$ and $\mathbf{P}(\mathbf{q})$ are the mass and the internal elastic force vector, and $\mathbf{P}_A(\mathbf{q})$ denotes the external forces by aerodynamic forces. The Newton–Raphson method combined with a line-search method was applied to improve convergence and reliability.

B. Transonic-Small-Disturbance Theory

The three-dimensional modified unsteady TSD equation may be written in conservation-law form as [14]

$$\frac{\partial f_0}{\partial t} + \frac{\partial f_1}{\partial x} + \frac{\partial f_2}{\partial y} + \frac{\partial f_3}{\partial z} = 0 \tag{5}$$

where

$$\begin{aligned} f_0 &= -A\phi_t - B\phi_x, \qquad f_1 = E\phi_x + F\phi_x^2 + G\phi_y^2 + G\phi_z^2 \\ f_2 &= \phi_y(1 + H\phi_x), \qquad f_3 = \phi_z \end{aligned} \tag{6}$$

The above equations are given in a physical coordinate system (x, y, z, and t), where the subscripts x, y, and z denote the derivative of each direction, and ϕ represents the disturbance velocity potential. The coefficients are defined as

$$\begin{aligned} A &= M^2, \qquad B = 2M^2, \qquad E = 1 - M^2 \\ F &= -\frac{1}{2}(\gamma + 1)M^2, \qquad G = \frac{1}{2}(\gamma - 3)M^2 \\ H &= -(\gamma - 1)M^2 \end{aligned} \tag{7}$$

where M is the freestream Mach number, and γ is the specific heat ratio. The coefficients depend on the assumptions made when deriving the TSD equation. Details of aerodynamic analysis schemes are discussed in Yoo et al. [15].

To couple a fluid flow solver with a structural solver directly, the transformation of forces and displacements between a finite element mesh and an aerodynamic grid should be introduced. For the displacements mapping onto a CFD grid, the cubic Lagrange shape functions are used. On the other hand, to transfer forces on a FEM mesh onto a CFD grid, the work-equivalent energy method is applied, which implies that the work done by virtual displacements and distributed forces is equal to that of virtual displacements and nodal forces. In a finite element model based on the large-deflection-beam theory, a global coordinate system differs from a deformed local coordinate system. However, in an aerodynamic model based on the TSD theory, these two coordinates coincide with each other. According to Patil and Hodges [7], the deviation of aerodynamic forces due to curvature effects can be negligible. Thus, the curvature effect is ignored, although three-dimensional aerodynamic forces are calculated by the TSD equation. Using a static aeroelastic analysis, the deformation of a wing can be obtained under the given static forces of gravity and steady aerodynamic forces. In addition, steady aerodynamic forces change according to the deformed shape. Thus, a converged deformation shape is calculated using an iterative

procedure. In the static equilibrium state, mode shapes and natural frequencies are obtained. After the static aeroelastic computation, the dynamic aeroelastic analyses are conducted.

III. Results and Discussion

A. Structural Analysis Under Gravity Loading

The planform of the high-aspect-ratio wing has a root chord length of 0.0508 m, a span length of 0.4508 m, and an aspect ratio of approximately 9. The NACA 0012 airfoil section was selected for the lifting surfaces. Additional details of the model along with the experimental procedures are discussed by Tang and Dowell [6]. For the structural analysis, five elements of a four-node cubic interpolation function are used. A clamped boundary condition is applied at the wing root.

Figure 2 shows comparisons of static deflections between the present results and the experimental data. Herein, theory results of reference are obtained by Hodges–Dowell equations [16]. The present numerical analysis results and experimental measurements of the tip deflections are compared for $\theta_0 = 0$, 45, and 90 deg. Flapwise bending refers to bending perpendicular to the wing chord, and chordwise bending refers to bending in the direction parallel to the wing chord. As the pitch angle increases, flapwise deflections decrease. On the other hand, chordwise deflections increase due to the geometrical bending-torsion coupling effect. The present numerical results for the flapwise and chordwise components show good agreement with the experimental data for all of the pitch angles in Figs. 2a and 2b. Similar results for the torsional deflection are illustrated in Fig. 2c. The characteristics of torsional deflection were sourced from the literature [17] and values of torsional deflections were calculated using the arc-cos formulation. The static tip deflections were in good agreement with the measured data. From comparisons of the present analysis results and the experimental data, the nonlinearity effects due to a large deflection are well described by the present nonlinear analyses. However, there is a slight difference between the linear and nonlinear analysis results under gravity-load effects.

Figure 3 shows the flapwise, chordwise, and torsional frequencies under gravity loading. The flapwise and chordwise frequencies show good agreement with the experimental data. With the increment of the pitch angle, the flapwise frequency slightly decreases. On the other hand, the chordwise frequency increases due to the stiffening effect. In the case of the torsional frequency, the present analysis results are slightly offset from the experimental data. However, the present nonlinear analysis results follow the variation of the natural frequencies as a function of the pitch angle. Thus, the present nonlinear analysis results accurately predict the static and dynamic behavior of the model of Tang and Dowell [6].

B. Aeroelastic Analysis Results

For the aerodynamic analysis, the grids contain $80 \times 78 \times 40$ points in the x, y, and z directions, respectively. Although the experimental model has a tip store, its aerodynamic effect is negligible [6]. Thus, the tip store is ignored in the aerodynamic analysis.

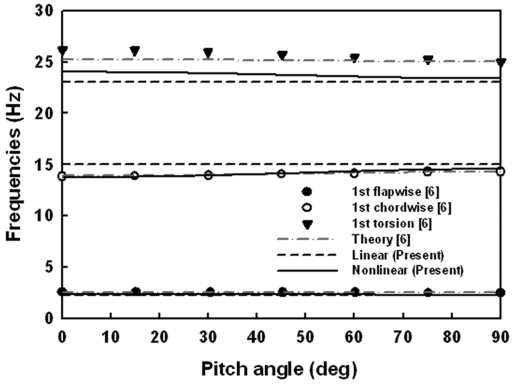

Fig. 3 Comparisons of natural frequencies under gravity loading.

The flapwise and twist deflections at the tip when the pitch angle of attack is 1.0 deg are presented in Fig. 4. Because of the aerodynamic forces, both the tip deflection and twist angle increase with the increment of the flow velocity. The balance between the aerodynamic and the gravity forces occurs at $U = 35$ m/s. This indicates that the aerodynamic forces provide sufficient aerodynamic force to overcome the effect of gravity. In general, the agreement of the twist deflection is excellent, except for a flow velocity of approximately 35 m/s. In the higher-velocity range, it was noted in a related study that the data fluctuation increases due to greater aerodynamic interference [6]. Moreover, it was noted that the present linear and nonlinear analysis results coincide because the current flow condition cannot sufficiently generate the geometric structural nonlinearity.

Figure 5 illustrates the static aeroelastic defections at the tip for the pitch angle of $\theta_0 = 2.2$ deg. The flapwise deflection is nearly equal to zero when the $U = 25$ m/s, as the aerodynamic force is equal to the gravity force. Similar to the case of $\theta_0 = 1.0$ deg, the deflections were increased with the increment of the velocity. However, the magnitude of the both the flapwise and twist deflections are larger than those of the lower pitch angle of attack, due to the increment of the external aerodynamic load. Several differences of deflections were also noted between the linear and nonlinear numerical results when $U = 35$ m/s. As can be seen in Fig. 5, it can be inferred that the geometric structural nonlinearity occurs over the velocity of 30 m/s.

Figure 6 shows the overall deformed shapes along the spanwise direction between the linear and nonlinear analysis results. When only the force of gravity is applied, the deformed shapes of the linear and nonlinear analysis cases are nearly identical. However, at a flow velocity of 35 m/s, the nonlinear analysis results show larger deflections for both the flapwise and twist deflections. In addition, the deflection of the axial direction is only found in the nonlinear case.

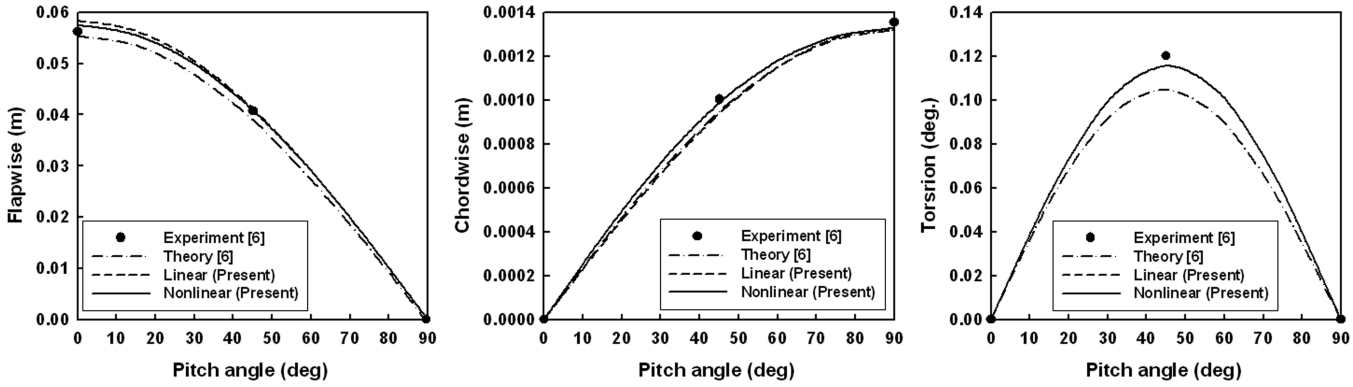

a) Flapwise **b) Chordwise** **c) Torsion**

Fig. 2 Comparisons of static deflections under gravity loading at the tip.

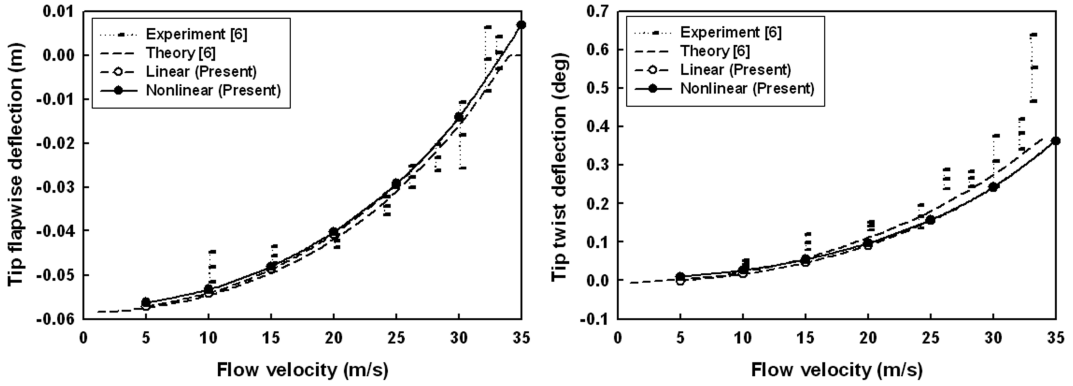

a) Flapwise deflection b) Twist deflection

Fig. 4 Static aeroelastic deflections at the pitch angle of attack of $\theta_0 = 1.0$ deg.

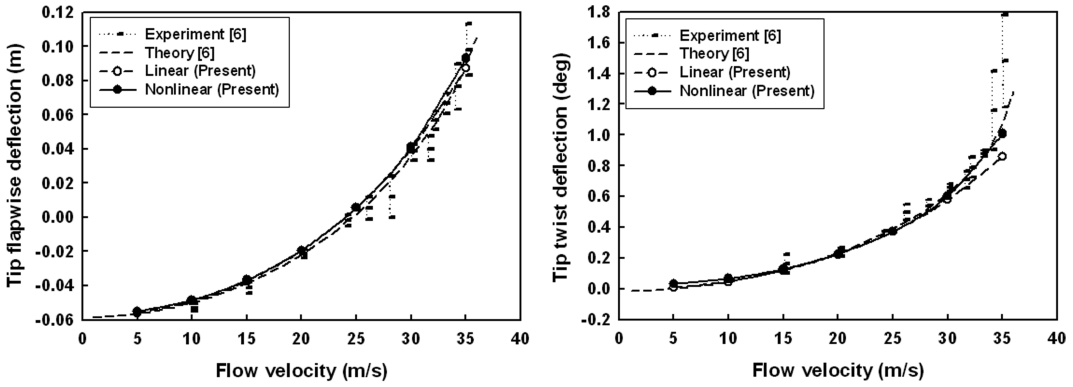

a) Flapwise deflection b) Twist deflection

Fig. 5 Static aeroelastic deflections at the pitch angle of attack of $\theta_0 = 2.2$ deg.

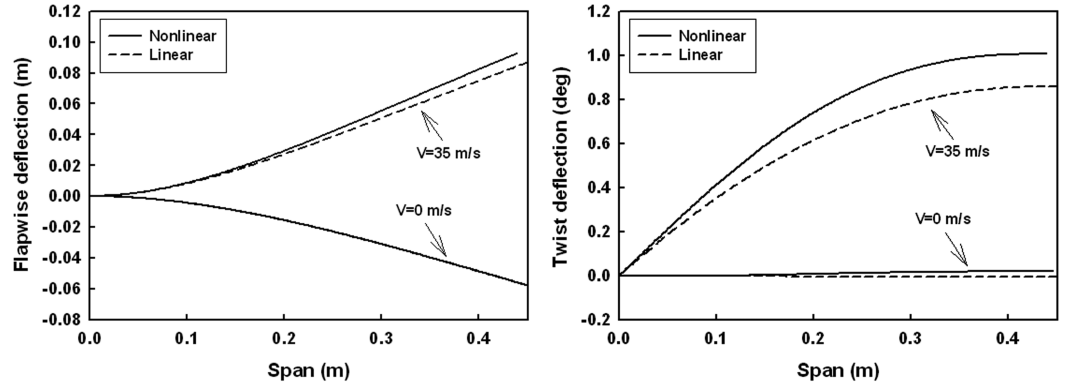

a) Flapwise deflection b) Twist deflection

Fig. 6 Comparisons of deformed shapes between linear and nonlinear cases at $\theta_0 = 2.2$ deg.

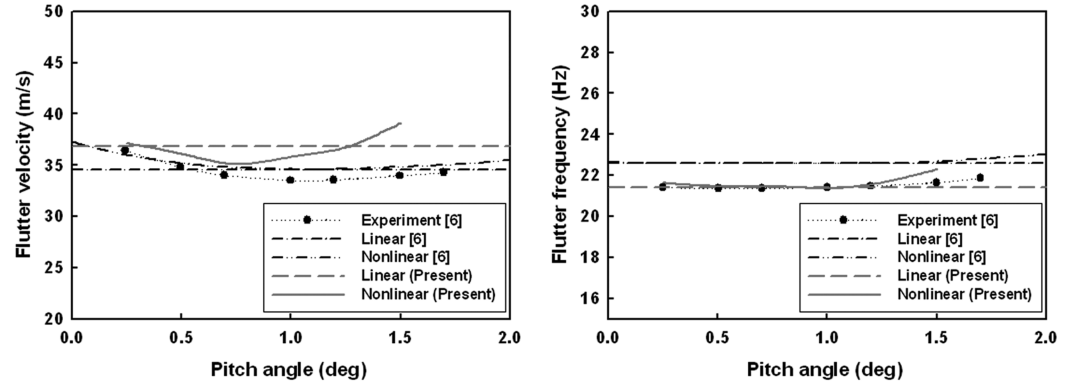

a) Flutter velocity b) Flutter frequency

Fig. 7 Flutter boundary of the wing model.

The dynamic flutter velocities and frequencies are shown in Fig. 7. For the prediction of the flutter boundary, as in the study of Tang and Dowell [6], a dynamic perturbation approach was used to determine the small-perturbation flutter boundary of this nonlinear analysis for a nonlinear static equilibrium condition. For comparison, the linear flutter boundary is also plotted. In the present analysis, the flutter velocities are higher than those of the reference data, whereas the flutter frequency shows good agreement. This difference is due to the aerodynamic model of the analysis results here compared with the reference data. In Tang and Dowell's [6] study, a dynamic stall model was used. However, the stall model is not considered in the present research. Therefore, the differences in the flutter velocity increase with high pitch angles. The present analysis results are in a good agreement with the experimental data in low-pitch-angle ranges.

IV. Conclusions

In this study, aeroelastic analyses of a high-aspect-ratio wing are conducted. To consider the geometrical nonlinearity of such a wing, the large-deflection-beam theory is introduced. Additionally, the transonic-small-disturbance theory is used for an efficient aerodynamic calculation. Conducting a structural analysis under a gravity effect, the structural analysis procedure and results of this study are verified. Static aeroelastic analyses are achieved using a structural solver based on the large-deflection-beam theory coupled with the TSD aerodynamic solver. The present research results were found to be in good agreement with the measured deflection data. The flutter boundaries are also presented using a small-perturbation approach. The developed nonlinear aeroelastic analysis method can efficiently predict flutter stability while taking into account geometrical structural nonlinearity.

Acknowledgments

This work was supported by the second stage of the Brain Korea 21 Project in 2009 and by the Defense Acquisition Program Administration and Agency for Defense Development under contract UD080041AD.

References

[1] van Schoor, M. C., and von Flotow, A. H., "Aeroelastic Characteristics of a Highly Flexible Aircraft," *Journal of Aircraft*, Vol. 27, No. 10, 1990, pp. 901–908. doi:10.2514/3.45955

[2] Pendaries, C., "From the HALE Gnopter to the Ornithopter—or How to Take Advantage of Aircraft Flexibility," Congress of the International Council of the Aeronautical Sciences, Paper A98-31715, Sept. 1998.

[3] Patil, M. J., Hodges, D. H., and Cesnik, C. E. S., "Nonlinear Aeroelasticity and Flight Dynamics of High-Altitude Long-Endurance Aircraft," *Journal of Aircraft*, Vol. 38, No. 1, 2001, pp. 88–94. doi:10.2514/2.2738

[4] Patil, M. J., Hodges, D. H., and Cesnik, C. E. S., "Limit-Cycle Oscillations in High-Aspect-Ratio Wings," *Journal of Fluids and Structures*, Vol. 15, No. ??, 2001, pp. 707–132. doi:10.1006/jfls.2000.0329

[5] Hall, B., Preidikman, S., Mook, D. T., and Nayfeh, A. H., "A Time-Domain Simulation for Evaluating Smart Wing Concepts for Reducing Gust Loads," *Proceedings of SPIE: The International Society for Optical Engineering*, Vol. 3668, No. 1, 1999, pp. 105–116. doi:10.1117/12.350687

[6] Tang, D. M., and Dowell, E. H., "Experimental and Theoretical Study on Aeroelastic Response of High-Aspect-Ratio Wings," *AIAA Journal*, Vol. 39, No. 8, 2001, pp. 1430–1441. doi:10.2514/2.1484

[7] Patil, M. J., and Hodges, D. H., "On the Importance of Aerodynamic and Structural Geometrical Nonlinearities in Aeroelastic Behavior of High-Aspect-Ratio Wings," *Journal of Fluids and Structures*, Vol. 19, No. 7, 2004, pp. 905–915. doi:10.1016/j.jfluidstructs.2004.04.012

[8] Smith, M. J., Patil, M. J., and Hodges, D. H., "CFD-Based Analysis of Nonlinear Aeroelastic Behavior of High-Aspect-Ratio Wings," AIAA Paper 2001-1582, 2001.

[9] Garcia, J. A., "Numerical Investigation of Nonlinear Aeroelastic Effects on Flexible High-Aspect-Ratio Wings," *Journal of Aircraft*, Vol. 42, No. 4, 2005, pp. 1025–1036. doi:10.2514/1.6544

[10] Bauchau, O. A., and Hong, C. H., "Nonlinear Composite Beam Theory," *Journal of Applied Mechanics*, Vol. 55, No. 1, 1988, pp. 156–163. doi:10.1115/1.3173622

[11] Stemple, A. D., and Lee, S. W., "Large Deflection Static and Dynamic Finite Element Analysis of Composite Beams with Arbitrary Cross Sectional Warping," AIAA Paper No. 89-1363-CP, 1989, pp. 1788–1798.

[12] Cho, M. H., and Lee, I., "Aeroelastic Stability of Hingeless Rotor Blade in Hover Using Large Deflection Theroy," *AIAA Journal*, Vol. 32, No. 7, 1994, pp. 1472–1477. doi:10.2514/3.12217

[13] Jeon, S. M., Cho, M. H., and Lee, I., "Static and Dynamic Analysis of Composite Box Beams Using Large Deflection Theory," *Computers and Structures*, Vol. 57, No. 4, 1995, pp. 635–642. doi:10.1016/0045-7949(95)00054-K

[14] Batina, J. T., "Efficient Algorithm for Solution of the Unsteady Transonic Small-Disturbance Equation," *Journal of Aircraft*, Vol. 25, No. 7, 1988, pp. 598–605. doi:10.2514/3.45629

[15] Yoo, J. H., Kim, D. H., Kwon, H. J., and Lee, I., "Nonlinear Aeroelastic Simulation of Full-Span Aircraft with Oscillating Control Surfaces," *Journal of Aerospace Engineering*, Vol. 18, No. 3, 2005, pp. 156–167. doi:10.1061/(ASCE)0893-1321(2005)18:3(156)

[16] Hodges, D. H., and Dowell, E. H., "Nonlinear Equations of Motion for the Elastic Bending and Torsion of Twisted Nonuniform Rotor Blades," NASA TN D-7818, 1974.

[17] Rosen, A., Loewy, R., and Mathew, M. B., "Nonlinear Analysis of Pretwisted Rods Using 'Principal Curvature Transformation'—Part 2: Numerical Results," *AIAA Journal*, Vol. 25, No. 4, 1987, pp. 598–604. doi:10.2514/3.9669